Second-order wave radiation by multiple cylinders in time domain through the finite element method

C.Z. Wang, S. Mitra and B.C. Khoo*

Department of Mechanical Engineering, National University of Singapore, 10 Kent Ridge Crescent, Singapore 119260, Singapore

Abstract. A time domain finite element based method is employed to analyze wave radiation by multiple cylinders. The nonlinear free surface and body surface boundary conditions are satisfied based on the perturbation method up to the second order. The first- and second-order velocity potential problems at each time step are solved through a finite element method (FEM). The matrix equation of the FEM is solved through an iteration and the initial solution is obtained from the result at the previous time step. The three-dimensional (3D) mesh required is generated based on a two-dimensional (2D) hybrid mesh on a horizontal plane and its extension in the vertical direction. The hybrid mesh is generated by combining an unstructured grid away from cylinders and two structured grids near the cylinder and the artificial boundary, respectively. The fluid velocity on the free surface and the cylinder surface are calculated by using a differential method. Results for various configurations including two-cylinder and four-cylinder cases are provided to show the mutual influence due to cylinders on the first and second waves and forces.

Keywords: second order wave radiation; time domain; multiple cylinders; finite element method; unstructured mesh.

1. Introduction

With the development of oil exploration and production in deep water, the design of offshore structures such as tension leg platforms (TLPs), semi-submersibles and drilling ships become interesting topics and has been studied for many years. In ocean environment, these structures are subjected to the actions of waves, winds and currents, which may produce nonlinear hydrodynamic forces on the structures and the corresponding nonlinear motions such as ringing or springing, slow drift and mean motions. Especially, these nonlinear loads and motions will be significant in severe environment.

The tension leg platform is the most common offshore structure suiting for deep-water operation. It mainly consists of a few columns and tendons for constraining the motion of the platform, and so a study on the intersection of waves and the structure with multiple bodies is very important. The perturbation method is a powerful tool to predict hydrodynamic forces and motions for offshore structures. There are lot of publications for wave-body interactions based on the perturbation method since the works of Lighthill (1979) and Molin (1979). The second order wave diffraction by multiple bodies can be found from those by Chau and Eatock Taylor (1992), Malenica, Eatock

*Corresponding author, Professor, E-mail: mpekbc@nus.edu.sg

Taylor and Huang (1999) in the frequency domain and Wang and Wu (2007) in the time domain. However, to the best knowledge of the authors, most of previous works are about the diffraction problems even for a single-body structure in three-dimension. Some works on second-order wave radiation problems may be found such as the oscillation of a single truncated cylinder by Li (1995) and Goren (1996) in the frequency domain and by Isaacson, Ng and Cheung (1993) in the time domain. Recently, Wang, Wu and Drake (2007) and Bai and Eatock Taylor (2009) simulated single non-wall-sided cylinders in forced motions based on the fully nonlinear wave potential theory. Simulations based on the fully nonlinear wave potential theory is good in describing large waves or motions in large amplitudes but need much more computer resources than the perturbation method.

The wave radiation by multi-body has many applications in ship and ocean engineering such as TLPs, semi-submersibles, floating airports and some special ships such as catamaran and SWATH (small waterplane area twin hull ship) that have two hulls and the interference may be important when advancing in waves. In addition, two or more vessels in sufficient proximity may have significant interactions. The earliest work on the radiation problem of multi-body is that by Ohkusu (1969) about heaving motions of two circular cylinders on free surface in two-dimension. Williams and Abul-Azm (1989) simulated wave radiation by a group of truncated cylinders, in which one cylinder underwent forced motions but others were fixed. They found the added mass and the damping coefficient of the cylinder are very different from that of a single isolated cylinder. Both these two works are based on the linear theory.

In the present paper, we study the second order wave radiation problems of multiple truncated cylinders in the time domain. The linear and second order waves and hydrodynamic forces are obtained by the finite element method and the interference between cylinders is investigated through changing the wave frequency and the spacing between cylinders.

2. Mathematical formulation

We consider the second order wave radiation problem by a group or an array of cylinders. As shown in Fig. 1, a right-handed Cartesian coordinate system *oxyz* is defined, in which x and y are measured horizontally and z points vertically upwards form the still water level. The *i*-th cylinder surface is denoted by S_{ib} ($i = 1, 2, \ldots, n$, where n is the cylinder number) and its unit normal vector directed outward from the fluid region is denoted by $\vec{N} = (N_{ix}, N_{iy}, N_{iz})$. The seabed is assumed horizontal along the plane $z = -h$. Let t denote time and η be the elevation of the free surface S_f relative to the still water level. When the fluid is assumed incompressible and inviscid, and the flow irrotational, the fluid motion can be described by a velocity potential ϕ which satisfies the Laplace equation within the fluid domain $\forall$

$$\nabla^2 \phi = 0 \quad \text{in } \forall \tag{1}$$

and is subject to the following boundary conditions

$$\frac{\partial \phi}{\partial z} - \frac{\partial \eta}{\partial t} - \frac{\partial \phi}{\partial x}\frac{\partial \eta}{\partial x} - \frac{\partial \phi}{\partial y}\frac{\partial \eta}{\partial y} = 0 \quad \text{on } S_f \tag{2}$$

$$\frac{\partial \phi}{\partial t} + g\eta + \frac{1}{2}|\nabla \phi|^2 = 0 \quad \text{on } S_f \tag{3}$$
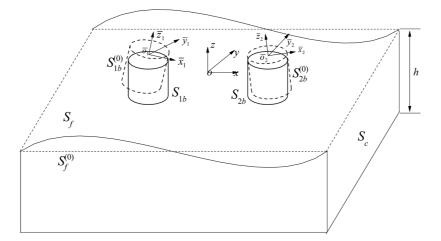
Fig. 1 A sketch of the problem

$$\frac{\partial \phi}{\partial N_i} = \vec{N}_i \cdot (\vec{V}_i + \vec{\Omega}_i \times \vec{r}_i) \qquad \text{on } S_{ib} \tag{4}$$

$$\frac{\partial \phi}{\partial N} = 0 \qquad \text{on } z = -h \tag{5}$$

where g is the acceleration due to gravity, $\vec{V}_i$ is the translational oscillatory velocity of the i-th cylinder and $\vec{\Omega}_i$ is the rotational velocity about a point on the i-th cylinder, which may be chosen as the mass centre of the body and $\vec{r}_i$ is the position vector from a point on the i-th body surface to the mass centre. In addition, the potential satisfies the radiation condition which is imposed through a suitable numerical procedure applied on a control surface S_c located at some distance away from the body as shown in Fig. 1.

One of the major difficulties in solving above-mentioned fully nonlinear free surface potential flow problems is the treatment of the free surface boundary conditions (2) and (3), which are both nonlinear and defined on the free surface which is not known prior to solving the problem. Here we will consider the problem to the second order. The second order approach for predicting floating structures has been given by Ogilvie (1983) in the frequency domain and then used by Isaacson, Ng and Cheung (1993) in the time domain.

Besides the coordinate system $oxyz$ shown in Fig. 1, we define another coordinate system $\bar{o}_i \bar{x}_i \bar{y}_i \bar{z}_i$, which is fixed on the i-th body and the origin $\bar{o}_i$ is located at the mass centre of the body $\vec{x}_{ig} = (x_{ig}, y_{ig}, z_{ig})$. The coordinates in systems $oxyz$ and $\bar{o}_i \bar{x}_i \bar{y}_i \bar{z}_i$ are denoted as $\vec{x} = (x, y, z)$ and $\vec{\bar{x}}_i = (\bar{x}_i, \bar{y}_i, \bar{z}_i)$ respectively. The unit normal vector of the mean body surface $S_{ib}^{(0)}$ directed outward from the fluid region is denoted by $\vec{n}_i = (n_{ix}, n_{iy}, n_{iz})$. The motion of the i-th rigid body can be described in terms of a translational motion vector $\vec{X}_i = (X_i, Y_i, Z_i)$ along the axis x, y and z and a rotational motion vector $\vec{\Theta}_i = (\Theta_{ix}, \Theta_{iy}, \Theta_{iz})$ around the mass centre. The displacement vector of a point on the i-th body surface is denoted by $\vec{\Xi}_i$ and it can be expressed as

$$\vec{\Xi}_i = \vec{x} - \vec{x}_{ig} - \vec{\bar{x}}_i \tag{6}$$

With the assumptions that the wave amplitude is small compared to the wavelength and the body motion is small compared to a principal body dimension, it is possible to apply Taylor series expansions to transform the free surface and body surface conditions, originally defined on the instantaneous surfaces, to conditions evaluated at the corresponding mean positions (Isaacson *et al.* 1993)

$$\left(\frac{\partial\phi}{\partial z}-\frac{\partial\eta}{\partial t}-\frac{\partial\phi}{\partial x}\frac{\partial\eta}{\partial x}-\frac{\partial\phi}{\partial y}\frac{\partial\eta}{\partial y}\right)+\eta\frac{\partial}{\partial z}\left(\frac{\partial\phi}{\partial z}-\frac{\partial\eta}{\partial t}-\frac{\partial\phi}{\partial x}\frac{\partial\eta}{\partial x}-\frac{\partial\phi}{\partial y}\frac{\partial\eta}{\partial y}\right)+\ldots = 0 \quad \text{on } S_f^{(0)} \tag{7}$$

$$\left(\frac{\partial\phi}{\partial t}+g\eta+\frac{1}{2}|\nabla\phi|^2\right)+\eta\frac{\partial}{\partial z}\left(\frac{\partial\phi}{\partial t}+g\eta+\frac{1}{2}|\nabla\phi|^2\right)+\ldots = 0 \quad \text{on } S_f^{(0)} \tag{8}$$

$$\dot{\vec{\Xi}}_i\cdot\vec{N}_i = [\nabla\phi+\vec{\Xi}_i\cdot\nabla(\nabla\phi)+\ldots]\cdot\vec{N}_i \quad \text{on } S_{ib}^{(0)}(i=1,2,\ldots,n) \tag{9}$$

where $S_f^{(0)}$ is the still water surface, $\dot{\vec{\Xi}}_i = \vec{V}_i+\vec{\Omega}_i\times\vec{r}_i$, where the over-dot indicates the time derivative. The boundary conditions may now be applied on $S_f^{(0)}, S_{ib}^{(0)}$ and other mean boundaries. Using the Stokes expansion procedure, quantities at first and second order are separated by introducing perturbation series for ϕ, η, $\vec{X}_i$ and $\vec{\Theta}_i$

$$\phi = \varepsilon\phi^{(1)}+\varepsilon^2\phi^{(2)}+\ldots \tag{10}$$

$$\eta = \varepsilon\eta^{(1)}+\varepsilon^2\eta^{(2)}+\ldots \tag{11}$$

$$\vec{X}_i = \varepsilon\vec{X}_i^{(1)}+\varepsilon^2\vec{X}_i^{(2)}+\ldots \tag{12}$$

$$\vec{\Theta}_i = \varepsilon\vec{\Theta}_i^{(1)}+\varepsilon^2\vec{\Theta}_i^{(2)}+\ldots \tag{13}$$

where ε is a perturbation parameter related to the wave slope which is small, and the superscripts (1) and (2) indicate respectively components at the first- and second-order. With assuming the motion to be harmonic and specified, $\vec{X}_i$ and $\vec{\Theta}_i$ may be considered to first order only, so that

$$\vec{X}_i = \varepsilon\vec{X}_i^{(1)} \tag{14}$$

$$\vec{\Theta}_i = \varepsilon\vec{\Theta}_i^{(1)} \tag{15}$$

which means $\vec{X}_i = (X_i^{(1)}, Y_i^{(1)}, Z_i^{(1)})$ and $\vec{\Theta}_i = (\Theta_{ix}^{(1)}, \Theta_{iy}^{(1)}, \Theta_{iz}^{(1)})$. For convenience, the superscript (1) will be omitted, so $(X_i^{(1)}, Y_i^{(1)}, Z_i^{(1)})$ and $(\Theta_{ix}^{(1)}, \Theta_{iy}^{(1)}, \Theta_{iz}^{(1)})$ can be denoted by (X_i, Y_i, Z_i) and $(\Theta_{ix}, \Theta_{iy}, \Theta_{iz})$ respectively.

Since we consider only small amplitude motions, the displacement $\vec{\Xi}_i$ can be expressed using the translational motion $\vec{X}_i$ and the rotational motion $\vec{\Theta}_i$ by the following equation

$$\vec{\Xi}_i = (\vec{X}_i+\vec{\Theta}_i\times\vec{x}_i)+\tilde{H}\vec{x}_i \tag{16}$$

where matrix $\tilde{H}$ is given as

$$\tilde{H} = \begin{bmatrix} -\dfrac{\Theta_y^2 + \Theta_z^2}{2} & 0 & 0 \\[2mm] \Theta_x \Theta_y & -\dfrac{\Theta_x^2 + \Theta_z^2}{2} & 0 \\[2mm] \Theta_x \Theta_z & \Theta_y \Theta_z & -\dfrac{\Theta_x^2 + \Theta_y^2}{2} \end{bmatrix}$$

Eq. (16) is valid up to second order. Similar to Eq. (16), the unit normal vector $\vec{N}$ is given by

$$\vec{N}_i = \vec{n}_i + \vec{\Theta}_i \times \vec{n}_i + \tilde{H}\vec{x}_i \tag{17}$$

By a time differentiation of Eq. (16), we obtain the velocity on the body surface

$$\vec{\Xi}_i = \left(\dot{\vec{X}}_i + \dot{\vec{\Theta}}_i \times \vec{x}_i\right) \times \dot{\tilde{H}}\vec{x}_i \tag{18}$$

Upon substituting the Stokes perturbation expansions of ϕ, η and $\vec{\Xi}_i$ into the Laplace equation and the boundary conditions and collecting terms of equal order, it yields the corresponding boundary-value problems for ε and ε^2 terms in the power series expansions, and so the boundary value problem at each order is now linear. In the k-th order wave radiation problem (with $k = 1$, 2 in turn), the potential satisfies the Laplace equation in the fluid domain $\forall^{(0)}$

$$\nabla^2 \phi^{(k)} = 0 \quad \text{in } \forall^{(0)} \tag{19}$$

and is subject to the boundary conditions applied on the still water surface, the mean body surface and the seabed, given respectively as

$$\frac{\partial \phi^{(k)}}{\partial z} - \frac{\partial \eta^{(k)}}{\partial t} = f_1^{(k)} \quad \text{on} \quad S_f^{(0)} \tag{20}$$

$$\frac{\partial \phi^{(k)}}{\partial t} - g\eta^{(k)} = f_2^{(k)} \quad \text{on } S_f^{(0)} \tag{21}$$

$$\frac{\partial \phi^{(k)}}{\partial n_i} = v_1^{(k)} \quad \text{on } S_{ib}^{(0)} \tag{22}$$

$$\frac{\partial \phi^{(k)}}{\partial z} = 0 \quad \text{on } z = -h \tag{23}$$

where $\forall^{(0)}$ is a time-independent fluid domain bounded by the seabed, the mean body surface $S_{ib}^{(0)}$, the still water surface $S_f^{(0)}$ and the open boundary S_c. The terms $f_1^{(k)}$, $f_2^{(k)}$, and $v_i^{(k)}$ are given respectively as

$$f_1^{(k)} = \begin{cases} 0 & (k=1) \\[2mm] \dfrac{\partial \phi^{(1)}}{\partial x}\dfrac{\partial \eta^{(1)}}{\partial x} + \dfrac{\partial \phi^{(1)}}{\partial y}\dfrac{\partial \eta^{(1)}}{\partial y} - \eta^{(1)}\dfrac{\partial^2 \phi^{(1)}}{\partial z^2} & (k=2) \end{cases}$$

$$f_2^{(k)} = \begin{cases} 0 & (k=1) \\ -\dfrac{1}{2}|\nabla\phi^{(1)}|^2 - \eta^{(1)}\dfrac{\partial^2\phi^{(1)}}{\partial z\partial t} & (k=2) \end{cases}$$

$$v_i^{(k)} = \begin{cases} \left(\dot{\vec{X}}_i + \vec{\Theta}_i\times\vec{\bar{x}}_i\right)\cdot\vec{n}_i & (k=1) \\ (\dot{\vec{H}}\vec{\bar{x}}_i)\cdot\vec{n}_i - \left[\left(\dot{\vec{X}}_i+\vec{\Theta}_i\times\vec{\bar{x}}_i\right)\cdot\nabla(\nabla\phi^{(1)})\right]\cdot\vec{n}_i \\ \quad + (\vec{\Theta}\cdot\vec{n}_i)\cdot\left[\left(\dot{\vec{X}}_i+\vec{\Theta}_i\times\vec{\bar{x}}_i\right)-\nabla\phi^{(1)}\right] & (k=2) \end{cases}$$

For the first order solution, the problem corresponds to the linear wave radiation problem; for the second order solution, the boundary problem is inhomogeneous and $f_1^{(2)}$, $f_2^{(2)}$ and $v_i^{(2)}$ represent quadratic forcings of the corresponding free surface and body surface conditions which can be determined from the first order solution.

The hydrodynamic forces on the i-th body can be obtained by carrying out a direct integration of the pressure over the instantaneous wetted body surface S_{ib}. The pressure in the fluid can be determined by the Bernoulli equation an can be written as

$$p = -\rho\left(\frac{\partial\phi}{\partial t}+\frac{1}{2}|\nabla\phi|^2+gz\right) \tag{24}$$

The hydrodynamic force acting on body can be expressed as

$$\vec{F}_i = \iint_{S_{ib}} p\vec{N}_i\,ds \tag{25}$$

where $\vec{\bar{r}}_i = \vec{\bar{x}}_i - \vec{\bar{x}}_{ig}$ is the vector from the point on the body surface to the mass centre. For the second order problem, the integration over the exact wetted body surface may be expressed as the sum of the integration over the mean wetted body surface and the correction integral defined at the still waterline *WL*. The hydrodynamic force contains three components

$$\vec{F}_i = \vec{F}_i^{(1)} + \vec{F}_i^{(2)} + \vec{F}_i^{(2)} \tag{26}$$

where $\vec{F}_i^{(1)}$, $\vec{F}_i^{(2)}$ and $\vec{F}_i^{(2)}$ are the first order oscillatory force at the excitation frequency, the second order oscillatory force at twice the excitation frequency and the second order mean force, respectively, on i-th body. $\vec{F}_i^{(1)}$ and $\vec{F}_i^{(2)}$ may be finally expressed as (Isaacson *et al.* 1993)

$$\vec{F}_i^{(1)} = \rho\iint_{S_{ib}^{(0)}}\frac{\partial\phi^{(1)}}{\partial t}\vec{n}_i\,ds - \rho g A_{iw}(Z_i^{(1)}+y_{if}\Theta_{ix}-x_{if}\Theta_{iy})\vec{k} \tag{27}$$

$$\vec{F}_i^{(2)} = \rho\iint_{S_{ib}^{(0)}}\frac{\partial\phi^{(2)}}{\partial t}\vec{n}_i\,ds - \frac{1}{2}\rho\iint_{S_{ib}^{(0)}}|\nabla\phi^{(1)}|^2\vec{n}_i\,ds - \frac{\rho g}{2}\oint_{WL}(\eta_r^{(1)})^2\vec{n}_l\,dl$$

$$-\rho \iint\limits_{S_{ib}^{(0)}} \left[((\vec{X}_i + \vec{\Theta}_i \times \vec{\bar{x}}_i)) \cdot \nabla\left(\frac{\partial \phi^{(1)}}{\partial t}\right) \right] \vec{n}_i ds - \rho \iint\limits_{S_b^{(0)}} \frac{\partial \phi^{(1)}}{\partial t} (\Theta_i \times \vec{n}_i) ds$$

$$-\rho g A_{iw} \left[(y_{if}\Theta_{iy}\Theta_{iz} + x_{if}\Theta_{iz}\Theta_{ix}) + \frac{1}{2}(\Theta_{ix}^2 + \Theta_{iy}^2)z_{ig} \right] \vec{k} - \vec{\bar{F}}_i^{(2)} \tag{28}$$

where A_{iw} is the mean waterplane area for i-th body, (x_{if}, y_{if}) is the centre of floatation in the system $oxyz$ when the i-th body is at rest, WL denotes the waterline. $\eta_r^{(1)} = \eta^{(1)} - Z_i - \Theta_{ix}\bar{y}_i + \Theta_{iy}\bar{x}_i$ is he relative wave height at the waterline for i-th body and $\vec{n}_l = \vec{n}/\sqrt{1-n_z^2}$. The mean force $\vec{\bar{F}}_i^{(2)}$ may be obtained by time averaging the part due to the first order potential in Eq. (28) over one period

$$\vec{\bar{F}}_i^{(2)} = -\rho \iint\limits_{S_{ib}^{(0)}} \overline{\frac{\partial \phi^{(1)}}{\partial t}(\vec{\Theta}_i \times \vec{n}_i)} ds + \frac{\rho g}{2} \oint\limits_{WL} \overline{(\eta_r^{(1)})^2 \vec{n}_l} dl - \rho \iint\limits_{S_{ib}^{(0)}} \overline{\left[\frac{1}{2}|\nabla \phi^{(1)}|^2 + (\vec{X}_i + \vec{\Theta}_i \times \vec{\bar{x}}_i) \cdot \nabla\left(\frac{\partial \phi^{(1)}}{\partial t}\right) \right] \vec{n}_i} ds$$

$$-\rho g A_{iw} \left[(y_{if}\Theta_{iy}\Theta_{iz} + x_{if}\Theta_{iz}\Theta_{ix}) + \frac{1}{2}(\Theta_{ix}^2 + \Theta_{iy}^2)z_{ig} \right] \vec{k} \tag{29}$$

The corresponding moment components $\vec{M}_i^{(1)}$, $\vec{M}_i^{(2)}$ and $\vec{M}_i^{(2)}$ may be obtained in the similar way and can be found in Isaacson, Ng and Cheung (1993),

3. Finite element discretization and numerical procedures

3.1 Finite element discretization

We use the finite element method here. A 2D mesh generator called BAMG (Hecht 1998) is used to generate the unstructured 2D grid (Fig. 2) on the plane first. It is then extended along the vertical direction to form the 3D mesh with prismatic elements, as shown in Fig. 3 for four truncated cylinders. The mesh on each cylinder is shown in Fig. 4.

The disturbance due the water waves usually decay very rapidly along the depth. It will therefore be more rational to use smaller elements near the free surface and larger elements near the bottom. Truncated cylinders are only considered here. We first divide the height between the free surface and the cylinder bottom into m_1 intervals using the following equation (Chung 2002)

$$z_i = \eta - (d+\eta) \frac{(2\alpha + \beta)\left(\frac{\beta+1}{\beta-1}\right)^{\frac{i/m_i - \alpha}{1-\alpha}} + 2a - \beta}{(2\alpha+1)\left[\left(\frac{\beta+1}{\beta-1}\right)^{\frac{i/m_i - \alpha}{1-\alpha}} + 1\right]} \quad (i = 0, 1, ..., m_1) \tag{30}$$

where z_i is the vertical coordinate of the element node at layer i and m is the number of layers. $\beta > 1$ in the equation is a constant. A smaller β will lead the elements to cluster near both the free
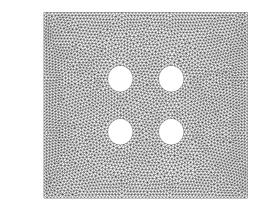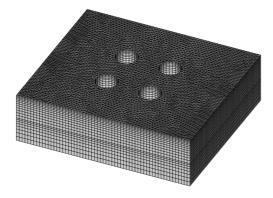
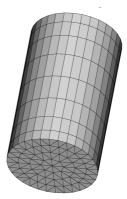Fig. 2 Mesh for four circles on the still water surface

Fig. 3 A 3D mesh for four truncated cylinders

Fig. 4 Mesh on a truncated cylinder surface

surface and the cylinder bottom, and a larger β will have the elements to distribute more uniformly along the depth. d is the draught of the cylinder and α is another constant. Eq. (32) can make the nodes and elements cluster at both the free surface and the cylinder bottom. We then divide the height between the cylinder bottom and the tank bottom into m_2 layers using the following equation (Chung 2002)

$$z_i = -d - (h-d)\frac{(\beta+1)-(\beta-1)\left(\frac{\beta+1}{\beta-1}\right)^{1-i/m_2}}{\left(\frac{\beta+1}{\beta-1}\right)^{1-i/m_2}+1}(i=0,1,\ldots,m_1)$$

(31)

In the present paper, β is taken as 1.05 in both Eqs. (30) and (31).

Once the mesh is generated, the potentials $\phi^{(k)} = (k=1,2)$ can be expressed in terms of the shape function $N_J(x,y,z)$

$$\phi^{(k)} = \sum_{j=1}^{n} \phi_J^{(k)} N_J(x,y,z)$$

(32)

where $\phi_J^{(k)}$ are the potentials at node J and n is the number of nodes. Based on the Galerkin method, we have

$$\iiint_{\forall^{(0)}} \nabla^2 \phi_J^{(k)} N_i \quad d\forall = 0 \tag{33}$$

Using Green's identity and the boundary conditions, we can obtain the following matrix equations

$$[K]\{\phi^{(k)}\} = \{F^{(k)}\}(k = 1, 2) \tag{34}$$

where

$$K_{IJ} = \iiint_{\forall^{(0)}} (\nabla N_I \cdot \nabla N_J) d\forall \qquad (I \notin S_p \ \& \ J \notin S_p)$$

$$F_I^{(K)} = \iint_{S_n} N_I f_n^{(k)} dS - \iiint_{\forall^{(0)}} \nabla N_I \sum_{\substack{j=1 \\ (J \in S_p)}}^{n} (f_p^{(k)})_J \nabla N_J d\forall \qquad (I \notin S_p)$$

S_p in above equations represents the Dirichlet boundary on which the potentials, denoted by $f_p^{(k)}$ $(k = 1,2)$, are known, and S_n represents the Neumann boundary on which the normal derivatives of the potentials, denoted by $f_p^{(k)}$ $(k = 1,2)$, are known. The matrix equations are then solved through an iteration based on the conjugate gradient method with a symmetric successive over relaxation (SSOR) preconditioner.

3.2 The evaluation of first- and second-order derivatives on the free surface and body surface

After the potential is found, its first and second order derivatives on element nodes are required to update $\eta^{(k)}$ and $\phi^{(k)}$ through Eqs. (20) and (21). The derivatives in theory can be obtained through the differentiation of the shape function. The accuracy is, however, usually not sufficient when the order of the shape function is low and the result becomes zero when the order of the derivative is higher than that of the shape function. Here we employ a cubic polynomial to express the velocity potential along straight mesh line in the vertical direction

$$\phi^{(k)} = a + bz + cz^2 + dz^3 \tag{35}$$

and its first- and second-order derivatives with respect to z $(k=1,2)$ are

$$w = \frac{\partial \phi^{(k)}}{\partial z} = b + 2cz + 3dz^2 \tag{36}$$

$$\frac{\partial^2 \phi^{(k)}}{\partial z^2} = 2c + 6dz \tag{37}$$

respectively, where a, b, c and d are coefficients and may be determined through solving the following system

$$\begin{bmatrix} 1 & z_1 & z_1^2 & z_1^3 \\ 1 & z_2 & z_2^2 & z_2^3 \\ 1 & z_3 & z_3^2 & z_3^3 \\ 1 & z_4 & z_4^2 & z_4^3 \end{bmatrix} \begin{bmatrix} a \\ b \\ c \\ d \end{bmatrix} = \begin{bmatrix} \phi_1^{(k)} \\ \phi_2^{(k)} \\ \phi_3^{(k)} \\ \phi_4^{(k)} \end{bmatrix}$$

where $z_i = (i = 1, 2, 3, 4)$ are four successive nodes along the vertical direction, and $\phi_i^{(k)}(i = 1,2,3,4)$ are the first- or second-order velocity potentials at z_i $(i = 1,2,3,4)$. The vertical velocity is obtained using Eq. (38). After the vertical velocity is obtained by Eq. (36), the following equation is used to obtain the horizontal components $\partial \phi^{(k)}/\partial x$ and $\partial \phi^{(k)}/\partial y$

$$\left.\begin{array}{l} \left(\dfrac{\partial \phi^{(k)}}{\partial x}\right)_i l_x^m + \left(\dfrac{\partial \phi^{(k)}}{\partial y}\right)_i l_y^m = \dfrac{\partial \phi^{(k)}}{\partial l^m} - \left(\dfrac{\partial \phi^{(k)}}{\partial z}\right)_i l_z^m \\[3mm] \left(\dfrac{\partial \phi^{(k)}}{\partial x}\right)_i l_x^n + \left(\dfrac{\partial \phi^{(k)}}{\partial y}\right)_i l_y^n = \dfrac{\partial \phi^{(k)}}{\partial l^n} - \left(\dfrac{\partial \phi^{(k)}}{\partial z}\right)_i l_z^n \end{array}\right\} (k = 1, 2) \tag{38}$$

where $\dfrac{\partial \phi^{(k)}}{\partial l^m} = \dfrac{\phi_{i+m} - \phi_i}{l^m}$, and $l_x^m, l_y^m, \& l_z^m$ are the components of $\vec{l}^{\,m}$ $(m=1,2,...)$, a vector formed by nodes $i+m$ and i. A weighted average was then used to obtain the final velocity. This method requires the node on the free surface and three nodes immediately below the free surface to be on the same vertical line. The method is found to be accurate but it is suitable only for wall-sided cylindrical structures.

In the first- and second-order body surface condition Eq. (22), some derivatives such as $\partial \phi^{(1)}/\partial x$, $\partial \phi^{(1)}/\partial y$, $\partial \phi^{(1)}/\partial z$, $\partial^2 \phi^{(1)}/\partial x^2$, $\partial^2 \phi^{(1)}/\partial y^2$, $\partial^2 \phi^{(1)}/\partial z^2$, $\partial^2 \phi^{(1)}/\partial x \partial y$, $\partial^2 \phi^{(1)}/\partial y \partial z$ and $\partial^2 \phi^{(1)}/\partial z \partial x$, are necessary. We can use the differential method to obtain these derivatives through interpolation. However, it may cause the result to be inaccuracy. Thus, we use a hybrid mesh on the free surface, in which a structured mesh in a torus shaped region is used near each cylinder as shown in shadow in Fig. 5. The structured mesh is obtained through discretized the torus by dividing it into some segments in tangential direction τ uniformly, which is clockwise and four segments in normal direction $\boldsymbol{n}$ directed toward the cylinder.

On the bottom of each cylinder, calculation of all first- and second-order derivatives is the same as those on the free surface.
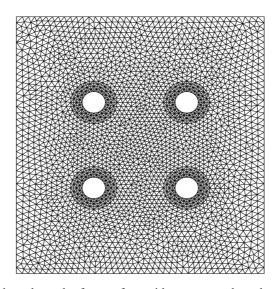

Fig. 5 The hybrid mesh on the free surface with a structured mesh near each cylinder

On the wall of the cylinder, the first- and second-order derivatives $\partial\phi/\partial n$ and $\partial^2\phi/\partial n^2$ along the normal direction n can be calculated through Eq. (36) by replacing z with the circle radius. Similarly, the tangential derivatives $\partial\phi/\partial\tau$ and $\partial^2\phi/\partial\tau^2$ may be obtained along the tangential direction τ. The derivative $\partial^2\phi/\partial n\partial\tau$ can be calculated by differencing $\partial\phi/\partial n$ along the tangential direction after obtaining $\partial\phi/\partial n$. All derivatives of potential with respect to x, y & z can be obtained through the following equations

$$\frac{\partial\phi^{(1)}}{\partial x} = \frac{\partial\phi^{(1)}}{\partial n}\frac{\partial n}{\partial x} + \frac{\partial\phi^{(1)}}{\partial s}\frac{\partial s}{\partial x} = \frac{\partial\phi^{(1)}}{\partial n}n_x + \frac{\partial\phi^{(1)}}{\partial s}n_y \tag{39}$$

$$\frac{\partial\phi^{(1)}}{\partial y} = \frac{\partial\phi^{(1)}}{\partial n}\frac{\partial n}{\partial y} - \frac{\partial\phi^{(1)}}{\partial s}\frac{\partial n}{\partial x} = \frac{\partial\phi^{(1)}}{\partial n}n_y - \frac{\partial\phi^{(1)}}{\partial s}n_x \tag{40}$$

$$\frac{\partial^2\phi^{(1)}}{\partial x^2} = \frac{\partial}{\partial x}\left(\frac{\partial\phi^{(1)}}{\partial x}\right) = \frac{\partial^2\phi^{(1)}}{\partial n^2}n_y^2 + 2\frac{\partial^2\phi^{(1)}}{\partial n\partial s}n_x n_y + \frac{\partial^2\phi^{(1)}}{\partial s^2}n_y^2 \tag{41}$$

$$\frac{\partial^2\phi^{(1)}}{\partial y^2} = \frac{\partial}{\partial y}\left(\frac{\partial\phi^{(1)}}{\partial y}\right) = \frac{\partial^2\phi^{(1)}}{\partial n^2}n_y^2 - 2\frac{\partial^2\phi^{(1)}}{\partial n\partial s}n_x n_y + \frac{\partial^2\phi^{(1)}}{\partial s^2}n_x^2 \tag{42}$$

$$\frac{\partial^2\phi^{(1)}}{\partial x\partial y} = \frac{\partial}{\partial y}\left(\frac{\partial\phi^{(1)}}{\partial x}\right) = \frac{\partial^2\phi^{(1)}}{\partial n^2}n_x n_y + \frac{\partial^2\phi^{(1)}}{\partial n\partial s}n_y^2 - \frac{\partial^2\phi^{(1)}}{\partial n\partial s}n_x^2 + \frac{\partial^2\phi^{(1)}}{\partial s^2}n_x n_y \tag{43}$$

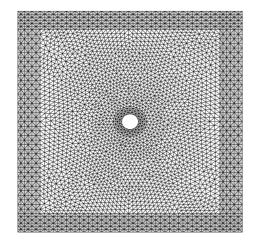### 3.3 Update potential and wave elevation on free surface

The fourth order Adams-Bashforth scheme is used to advance the simulation through time stepping method

$$f(t+\Delta t) = f(t) + \frac{\Delta t}{24}[55f'(t) - 59f'(t-\Delta t) + 37f'(t-2\Delta t) - 9f'(t-3\Delta t)] \tag{44}$$

where $f(t)$ represents either the velocity potential or wave elevation on the free surface. This scheme provides a high order accuracy and is particularly suited for the solution based on the perturbation procedure. As the mesh is fixed and no remeshing is applied throughout the simulation, the information including wave elevation, potential and velocity at previous time steps can be stored easily.

3.4 Absorbing boundary conditions

For long time simulations, an appropriate radiation condition should be imposed on the boundary S_c to minimize the wave reflection. Here we use a combination of Sommerfeld-Orlanski condition and a damping zone. The Sommerfeld-Orlanski condition used is based on that in Issacson and Cheung (1993). In order to use this condition, we used a structured mesh near the boundary S_c (see Fig. 6), the potential and velocity on the node of the structured mesh can be calculated directly. Otherwise, interpolation is necessary and it may cause accuracy to be lost. The damping zone adopted is similar to that used by Nakos *et al*. (1993) for the linear problem. We rewrite Eq. (20) as
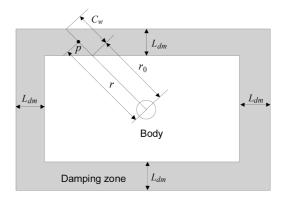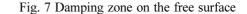
Fig. 6 An structured mesh near the control surface S_c

Fig. 7 Damping zone on the free surface

$$\frac{\partial \eta^{(k)}}{\partial t} = \frac{\partial \phi^{(k)}}{\partial z} - f_1^{(k)} - 2\nu \eta^{(k)} + \frac{\nu^2}{g} \phi^{(k)} \quad (k = 1, 2) \qquad \text{on } z = 0 \tag{45}$$

where ν is the damping coefficient given by

$$\nu(r) = 3\frac{C_s}{C_w^3}(r - r_0)^2 \quad 0 \leq r - r_0 \leq C_w. \tag{46}$$

r in Eq. (46) is the distance for the point under consideration to the centre of the nearest cylinder. For the single body shown in Fig. 7, damping zone starts from the edge of an inner rectangle $r = r_0(x, y)$ and ends at outer rectangle $r = r_0(x, y) + C_w(x, y)$. C_s in the equation is a constant to control the strength of the damping coefficient and is chosen to be 1.0 in this study, and the width of the damping zone L_{dm} (see Fig. 7) is set to be one wavelength for short waves and eight times the radius of the cylinder for long waves.

4. Numerical results

In the numerical simulation, a modulation function $M(t)$ is applied in body surface boundary condition (22) in order to let the wave develop gradually (Isaacson *et al*. 1993)

$$\frac{\partial \phi_D^{(k)}}{\partial n} = -M(t)\frac{\partial \phi_I^{(k)}}{\partial n} \quad (k = 1, 2) \tag{47}$$

where

$$M(t) = \begin{cases} \frac{1}{2}\left[1 - \cos\left(\frac{\pi t}{T}\right)\right] & t < T \\ 1 & t \geq T \end{cases}$$

and $T = 2\pi/\omega$ is the wave period. The use of the modulation function helps the wave to reach the

periodic state more smoothly and quickly.

4.1 Single cylinder case

We first consider a single truncated cylinder in vertical motions. The water depth is $h = a$, where a is the radius of the cross section of each cylinder and the height of the cylinder is $d=h/2$. The cylinder is subject to the following harmonic motion in the vertical direction

$$Z = A\sin\omega t \tag{48}$$

where A and ω is the oscillatory amplitude and frequency of the motion, respectively. In the simulation, $A=0.1a$. This case has been studied by Li (1995) and Goren (1996) in the frequency domain.

We consider a case with a nondimensional wavenumber $k_0a=1.0$ (k_0 is wavenumber in finite water depth and $\omega = \sqrt{k_0 g \tanh(k_0 h)}$. In the vertical direction, the height of elements near the free surface and the bottom should be small enough and this may be achieved by Eq. (32), by which we divide the height of the cylinder into 12 layers. Similarly, the height between the cylinder bottom and sea bottom is divided 10 layers according to Eq. (33). There are 40 segments along the cross section of each cylinder. On the free surface, both length and width of the domain are $40a$ and there is 128 intervals along both directions of length and width, which corresponds to 16532 nodes and 32560 triangular elements. In the simulation, the modulation function will be used. The time interval is $T/200$ ($T = 2\pi/\omega$). The corresponding history of vertical force is shown in Fig. 8. The force nonlinearity is very clear.

The amplitude of the first order force versus the nondimensional wavenumber k_0a is shown in Fig. 9. It is seen that the present numerical results are in very good agreement with those by Li (1995) and Goren (1996) in the frequency domain. The amplitudes of the two second order force components $F^{(21)}$ and $F^{(22)}$ corresponding to the contributions from the first- and second-order potentials, respectively, are given in Fig. 10. Generally, $F^{(21)}$ is smaller than those by Li (1995) and Goren (1996) and $F^{(22)}$ is between them. The total second order force $F^{(2)}$ and the mean force $\overline{F}^{(2)}$ are given in Fig. 11. It is shown that $F^{(2)}$ is in very good agreement with Goren's (1996) result, and the mean forces obtained by the three methods are nearly identical, which confirms that the present numerical method is efficient and accurate.
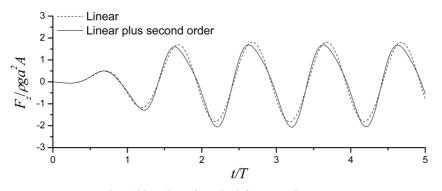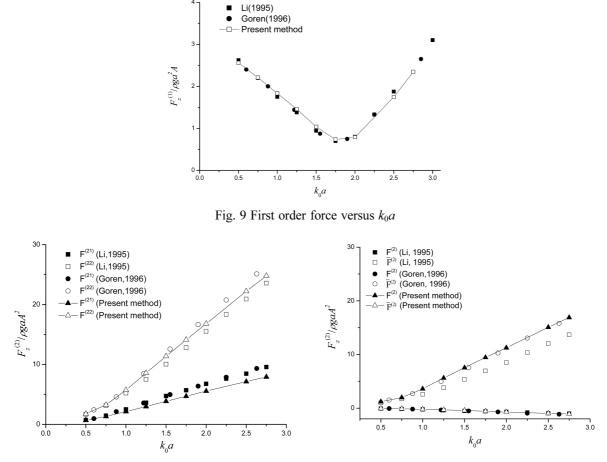

Fig. 8 histories of vertical forces at $k_0a = 1.0$

Fig. 9 First order force versus k_0a

Fig. 10 Second order force components versus k_0a

Fig. 11 Toal second order force and mean force versus k_0a

4.2 Two-cylinder case

We next consider wave radiation by two identical cylinders in vertical motions given by Eq. (48). The dimension of each cylinder is the same as the above single cylinder. The spacing between the two cylinders is $L_{cy} = 4a$. The centre of section of each cylinder is on $y = 0$, and cylinder 1 & 2 are located at $(-2a,0)$ and $(2a,0)$, respectively. We consider cylinder 1 only because of symmetry. The nondimensional wavenumber is $k_0a = 1.0$ and water depth $h = a$. The second order wave on the left and right sides of cylinder 1 are given in Fig. 12. It is seen that the development of the waves is very good and in stable periodic state within 20 cycles. The linear and linear plus second order waves are shown in Fig. 13 and the nonlinear feature can be clearly seen. A comparison of the linear and second order waves between this two-cylinder case and a single isolated cylinder case by removing cylinder 2 is shown in Fig. 14. It is seen that both linear and second order waves at the right side in the two cases are different in phase and amplitude. The waves at the left side are slightly different for linear wave but almost identical for the second order. The comparison of linear and second order forces in the vertical direction is given in Fig. 15. It seems that the difference between the two cases is very small. Fig. 16 shows the history of the hydrodynamic force. It is seen
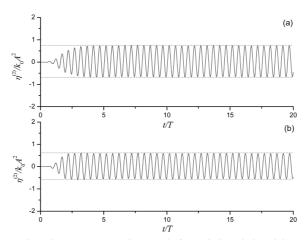
Fig. 12 Histories of second order waves at the (a) left and (b) right sides of cyilnder 1 at $k_0a = 1.0$
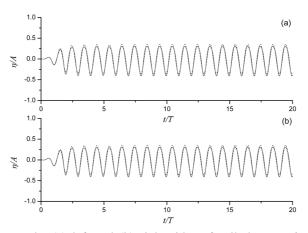

Fig. 13 Histories of waves at the (a) left and (b) right sides of cyilnder 1 at $k_0a = 1.0$ ········ linear; —— linear plus second order
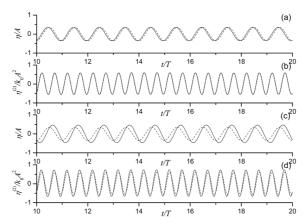

Fig. 14 Comparisons of linear and second order waves at the (a), (b) left and (c), (d) right sides of cyilnder 1 at $k_0a = 1.0$ —— two-cylinder case; ········single isolated cylinder case
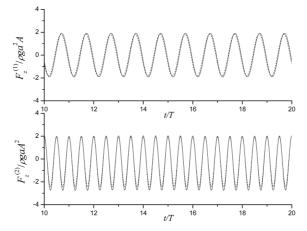
Fig. 15 Comparisons of linear and second order forces at $k_0a = 1.0$ ——two-cylinder case; ········ single isolated cylinder case

Fig. 16 Histories of hydrodynamic force on cylinder 1 at $k_0a = 1.0$ ········ linear; —— linear plus second order
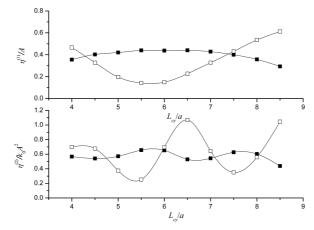

Fig. 17 Linear and second order waves for clinder 1 versus spacing between both cylinders at $k_0a = 1.0$; ——■—— left side ——□—— right side

that the nonlinearity is clear for the component in *z*-direction.

The difference at different frequencies is clearly seen. Fig. 17 shows that first and second order waves for cylinder 1 vary with the spacing between both cylinders. It is seen that both first and second order waves at the left side change slowly with the spacing but those at the right side are more affected by the spacing. The maximum wave amplitude at the right side is much larger than that at the left side for both linear and second order waves. The corresponding force versus k_0a is given in Fig. 18. Generally, the effect of spacing on vertical force and its components is smaller. In the horizontal direction, the spacing has an important influence on the second order force $F_x^{(2)}$ and the component due to the second order potential $F_x^{(22)}$, and the influence on the second order mean force $\overline{F}_x^{(2)}$ is also clear. Fig. 19 shows the snapshot of the wave profile around the cylinders at t/T=19. The nonlinear feature of the wave can be observed from the figure.
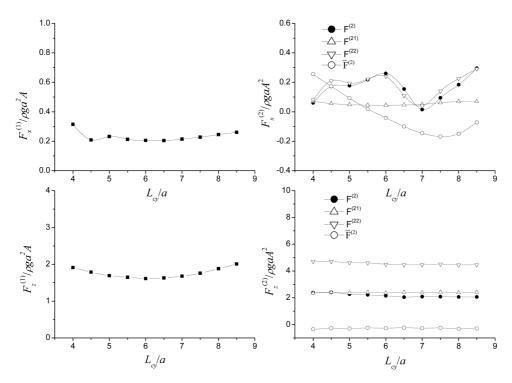

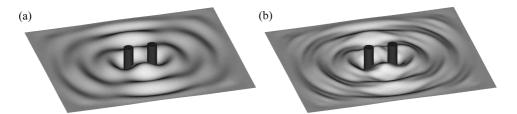Fig. 18 Linear and second forces on cylinder 1versus spacing between both cylinders at $k_0a = 1.0$

Fig. 19 Wave profiles at $t/T = 19$ ($k_0a = 1.0$ and $L_{cy} = 5a$) in vertical motions (a) linear and (b) linear plus second order

Simulations are also made for two cylinders in swaying motions, and the detailed results will be presented in the conference.

4.3 Four-cylinder case

Finally, we discuss some four-cylinder cases. The water depth $h = 3a$ and the cylinder height $d = h/2$. All cylinders are in identically vertical motions described by Eq. (48). The configuration is symmetric about both x- and y-axes and cylinders 1 & 2 are located ($-2a$, $-2a$) & ($2a$, $-2a$), respectively. The nondimensional wavenumber is $k_0a=1$ and the oscillational amplitude $A=0.1a$. Firstly, a case of vertical motions is simulated. The waves on the left and right sides of cylinder 1 are given in Fig. 20. It seems that the wave nonlinear feature is weak. The hydrodynamic force is, however, has stronger nonlinearity for components in both x- and z-direction as shown in Fig. 21. Fig. 22 shows a snapshot of wave profiles at $t/T=19$. The case of all four cylinders in identical horizontal motions (48) is also considered and Fig. 23 shows f wave profiles at $t/T=19$ and it is seen that the effect of the second order wave is important .
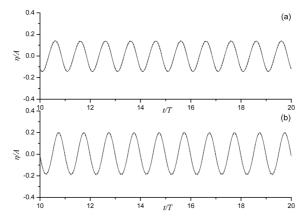

Fig. 20 Histories of waves at the (a) left and (b) right sides of cyilnder 1 at $k_0a = 1.0$ ········ linear; —— linear plus second order
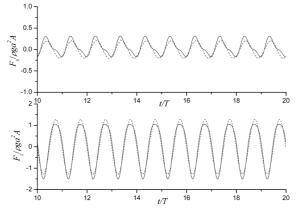

Fig. 21 Histories of hydrodynamic force on cylinder 1 at $k_0a = 1.0$ ········ linear; —— linear plus second order
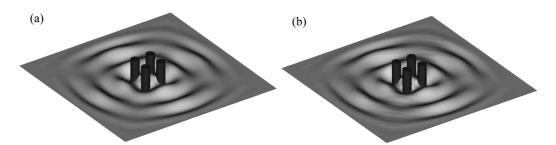
(a) (b)

Fig. 22 Wave profiles at $t/T = 19$ in vertical motion (a) linear and (b) linear plus second order
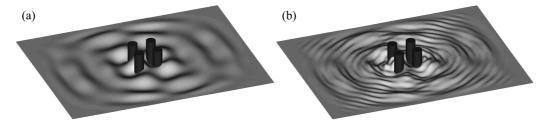
(a) (b)

Fig. 23 Wave profiles at $t/T = 19$ in horizontal motion (a) linear and (b) linear plus second order

5. Conclusions

A finite element based numerical method has been employed to study second order wave radiation by multiple truncated cylinders in open seas. The 3D mesh is obtained through an extension of a 2D hybrid mesh linked by a Delaunay unstructured grid and two structured grids near the cylinder and the truncated artificial boundary, respectively. The finite element method was employed to calculate the velocity potential in the fluid domain and the differential method is used to calculate the velocity on the free surface and body surface.

A truncated vertical cylinder undergoing forced sinusoidal oscillations was first selected to validate the present numerical method, the time histories of wave elevation and hydrodynamic forces at first and second order on the cylinder are calculated and the result of first and second order forces have been compared with previous studies and good agreement have been achieved.

Two-cylinder cases are then studied. Steady state solutions are achieved over a long duration in terms of the first and second order waves. The amplitudes of first and second forces vary with the spacing between both cylinder are discussed and comparisons are made with those in single isolated cylinder cases. Results show that both first and second order waves in the region between cylinders may be more affected by the interference. For the horizontal force, the total second order force $F_x^{(2)}$ and the component $F_x^{(22)}$ may change quickly with the spacing. The vertical force and its components are, however, are generally slightly affected by the spacing.

A four-cylinder case is also been investigated and more work is needed for further study, which includes more analyses of the effect of oscillational frequency and cylinder spacing on the first and second order waves and forces, and more simulations of wave radiation by larger arrays of cylinders are also under consideration.

Acknowledgements

References

Bai, W. and Eatock Taylor, R. (2006), "Higher-order boundary element simulation of fully nonlinear wave radiation by oscillating vertical cylinders", *Appl. Ocean Res.*, **28**(4), 247–265.

Chau, F.P. and Eatock Taylor, R. (1992), "Second-order wave diffraction by a vertical cylinder", *J. Fluid Mech.*, **240**, 571-599.

Chung, T.J. (2002), *Computational Fluid Dynamics*, Cambridge University Press.

Goren, O. (1996), "On the second-order wave radiation of an oscillating vertical circular in finite-depth water", *J. Ship Res.*, **40**(3), 224-234.

Hecht, F. (1998), "BAMG: Bidimensional anisotropic mesh generator", Website: http://www-rocq1.inria.fr/gamma/cdrom/www /bamg/eng.htm.

Isaacson, M., Ng, J.Y.T. and Cheung, K.F. (1993), "Second-order wave radiation of three-Dimensional bodies by time-domain method", *Int. J. Offshore Polar.*, **3**(4), 264-272.

Li, Y. (1995), *Simulation of 3D nonlinear wave-structure interaction in a numerical wave basin*, Ph.D. Thesis, Tech. Univ. of Nova Scotia Halifax.

Lighthill, M.J. (1979), "Waves and hydrodynamic loading", *Proceedings of the 2nd International Conference on the Behaviour of Offshore Structures*, London.

Malenica, S., Eatock Taylor, R. and Huang, J.B. (1999), "Second order water wave diffraction by an array of vertical cylinders", *J. Fluid Mech.*, **390**, 349-373.

Molin, B. (1979), "Second order diffraction loads upon three-dimension bodies", *Appl. Ocean Res.*, **1**, 197-202.

Nakos, D.E., Kring, D., Sclavounos, P.D. (1993), "Rankine panel methods for transient free surface flows", *Proceedings of the 6th International Conference on Numerical Ship Hydrodynamics*, Iowa.

Ohkusu, M. (1969), "On the heaving motion of two circular cylinders on the surface of a fluid", *Reports of Research Institute for Applied Mechanics*, **17**(58), 167-185.

Wang, C.Z. and Wu, G.X. (2007), "Time domain analysis of second order wave diffraction by an array of vertical cylinders", *J. Fluids Struct.*, **23**(4), 605-631.

Wang, C.Z., Wu, G.X., Drake, K.R. (2007), "Interactions between fully nonlinear water wave and non-wall-sided structures", *Ocean Eng*, **34**(8-9), 1182-1196.

Williams, A.N. and Abul Azm, A.G. (1989), "Hydrodynamic interactions in floating cylinder array-II. Wave radiation", *Ocean Eng*, **16**, 217-263.